

Article

Carbon Deposition Behavior of Ni Catalyst Prepared by Combustion Method in Slurry Methanation Reaction

Keming Ji ^{1,2}, Fanhui Meng ^{2,*}, Jiayao Xun ¹, Ping Liu ¹, Kan Zhang ^{1,*}, Zhong Li ² and Junhua Gao ¹

¹ State Key Laboratory of Coal Conversion, Institute of Coal Chemistry, Chinese Academy of Sciences, 27 South Taoyuan Road, Taiyuan 030001, China

² Key Laboratory of Coal Science and Technology of Ministry of Education and Shanxi Province, Taiyuan University of Technology, Taiyuan 030024, China

* Correspondence: mengfanhui@tyut.edu.cn (F.M.); sxicc602@163.com (K.Z.); Tel.: +8613935154736 (F.M.); +8618935139248 (K.Z.)

Received: 30 April 2019; Accepted: 25 June 2019; Published: 28 June 2019



Abstract: Ni/Al₂O₃ catalyst prepared by combustion method was applied in a slurry methanation reaction to study the catalytic performance, especially the regeneration performance. The catalyst properties were characterized by (X-Ray diffraction) XRD, Inductively coupled plasma atomic emission spectrometer (ICP-AES), Nitrogen adsorption-desorption, Transmission electron microscopy (TEM), Thermogravimetric analysis (TG/DTG), Temperature programmed oxidation (TPO), and H₂ chemisorption before and after reaction. The results show that the catalyst deactivation was mainly due to carbon deposition, which exhibited amorphous carbon films and formed by the disproportionation of CO. The carbon deposition was formed on the catalyst surface and existed as carbon films during the reaction, then it gradually separated from the catalyst surface, generated an overlapping multi-layer three-dimensional carbon structure, which covered the active site and blocked the pores. As a result, the metal surface area of catalyst decreases, as well as the activity. The carbon deposition could be removed by oxidative calcination without destroying the catalyst structure, the active sites could be re-exposed and the catalyst activity could be recovered.

Keywords: carbon deposition; catalyst deactivation; Ni catalyst; slurry-bed reactor; catalyst regeneration

1. Introduction

Coal is the most abundant fossil energy on Earth, which can be used to prepare coke [1], aromatics [2], methane [3–5], methanol [6], ammonia [7], gasoline [8] and other chemical products through coking, gasification and liquefaction. Among them, the process of coal gasification to methane has been extensively studied in recent years [9–11], due to its high energy conversion efficiency, short process flow and low equipment investment of unit product.

Syngas (CO+H₂) methanation is the key technology for coal to methane, mostly using Ni-based catalyst. However, methanation is a strong exothermic reaction, 1% of the CO conversion could cause 74 °C adiabatic temperature rise [12]. The reactor bed is likely to overheat, leading to rapidly sintered catalyst. For a slurry-bed reactor with inert liquid medium, the heat reaction could be removed in time by the liquid paraffin wrapped catalyst, which could solve the problem of overheating in the bed. Hence, researchers have paid more attention to the slurry-bed methanation reaction process, the reaction temperature, pressure, velocity and other reaction process [13,14]. In addition, the structure and properties of the catalyst [15–18] have been systematically studied, and it was found that the preparation method can significantly affect the specific surface area, Ni particle size, dispersion and

adsorption properties of the catalyst. Among them, the catalyst prepared by combustion method has a large specific surface area, small particle size and uniform dispersion of Ni. Furthermore, it has a large active metal surface area [19,20]. Under the conditions of 300 °C, 1.0 MPa, 3000 mL·g⁻¹·h⁻¹, the CO conversion and the CH₄ selectivity reaches 94.3% and 93.7%, respectively [21]. In our previous studies, combustion method has been applied in slurry phase methanation reaction, the influence of Ni contents [21], precursor of supports [22], type of fuels [23] and other key influence factors on catalytic performances have been systematic researched.

Besides CO conversion and CH₄ selectivity, stability is another key catalytic indicator. The primary reason for the stability and the deactivation of Ni catalyst is the carbon deposition of Ni [24]. At present, there are a large number of studies on the mechanism of carbon deposition [25], the structure of carbon deposition [26], the influence of carbon deposition on the activity of catalyst [27–30]. In the methanation reaction, the carbon deposition is mainly derived from the disproportionation of CO and decomposition of CH₄. On the catalyst surface, the formation of a variety of morphologies of the amorphous carbon, part of the crystallization of carbon and graphite carbon, ultimately lead to Ni sintering, pore blockage, or active center covered, resulting in catalyst deactivation. The carbon deposition behavior of the catalyst is affected by a variety of factors such as reactor [31], temperature, pressure and other technological conditions [32], such as the structure and properties of the catalyst [33]. To our best knowledge, the catalyst regeneration and carbon deposition behavior for CO methanation in a slurry-bed reactor has not been reported.

In this study, Ni/Al₂O₃ catalyst was prepared by combustion method. The catalytic stability and regeneration properties were investigated in a low-temperature slurry-bed reactor. Furthermore, the catalyst and its carbon deposition are characterized, as are the structure and properties of carbon deposition. The effects of carbon deposition on catalyst properties and catalytic performance are also discussed.

2. Results

2.1. Catalytic Stability Evaluation in Slurry-bed

The results of assessment of the Ni/Al₂O₃ catalyst in the slurry-bed methanation system are shown in Figure 1. At the first 20 h of the reaction, the CO conversion and CH₄ selectivity increase, up to 91.3% and 92.9%, respectively. After a reaction time of 450 h, the CH₄ selectivity remains around 92%, indicating that CH₄ is the main product in the slurry-bed methanation reaction with a stable selectivity during the reaction. Meanwhile, the CO conversion decreases to 69.1% and the deactivation rate is 0.053% h⁻¹. It was reported that the catalyst deactivation rate in the fixed-bed methanation system is 0.075% h⁻¹ [34], 0.113% h⁻¹ [35], 0.130% h⁻¹ [36] and 0.360% h⁻¹ [37]. Obviously, in the slurry-bed methanation system, the catalyst deactivation is slower and the stability is better than that of the fixed-bed system.

After the reaction, the catalyst was calcined in air atmosphere at 400 °C for 4 h to remove the carbon deposition, which may be present in the catalyst and then regenerated. The evaluation results of the catalyst after regeneration are shown in Figure 1b. The result shows that, in a reaction time of 100 h, the average CO conversion and CH₄ selectivity of refreshed catalyst reaches 89.6% and 91.8%, respectively. Then, the CO conversion gradually decreases. After a reaction time of 250 h, the CO conversion falls to 80.5%, which is very closed to that of fresh catalyst, indicating that after the regeneration process, the catalyst performance is almost fully recovered.

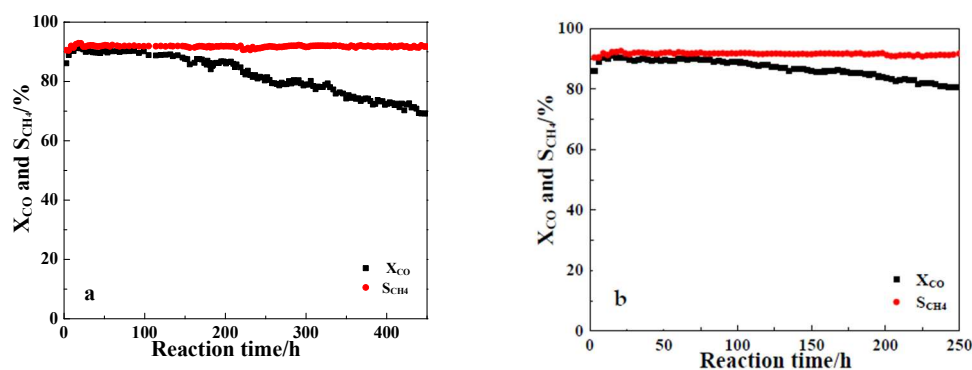


Figure 1. CO conversion and CH₄ selectivity of fresh catalyst (a) and refreshed catalyst (b) in slurry-bed reactor.

2.2. Catalyst Composition

The XRD characterization of the catalyst is shown in Figure 2. The characteristic diffraction peaks of Ni and γ -Al₂O₃ can be observed in the fresh catalyst, indicating that the Ni phase is formed in the process of catalyst preparation and Al₂O₃ phase of the support is maintained. The diffraction peak of γ -Al₂O₃ is still presented in the catalyst, but the intensity of Ni is weaker than that of fresh catalyst, and gradually decreases with increasing reaction time. The diffraction peak of Ni is not observed in the catalyst after 450 h. The decrease of Ni intensity indicates that the ordering of the Ni grains in the catalyst is deteriorated, which is related to the accumulation of carbon. The results show that the active carbon deposition firstly produced in the reaction can be dissolved in Ni particles, partially form carbonized nickel [26].

The XRD patterns of the catalyst after regeneration is also shown in Figure 2. It can be seen that the peak intensity of γ -Al₂O₃ and Ni in the catalyst after regeneration, is very close to that of the fresh catalyst.

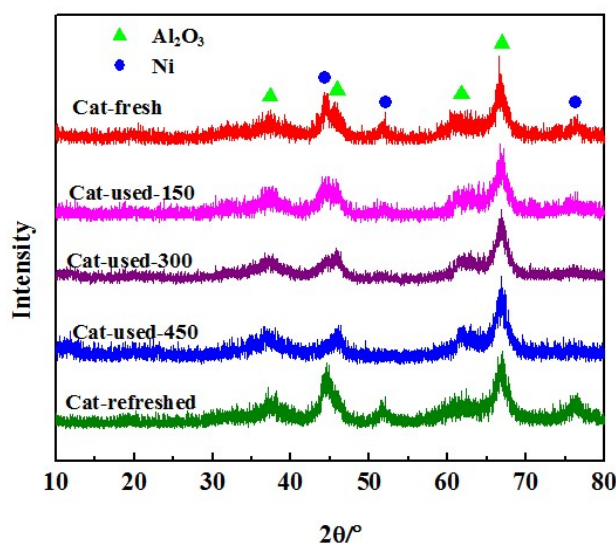


Figure 2. X-Ray diffraction patterns of catalysts.

The results of the Inductively coupled plasma atomic emission spectrometer characterization of the catalyst are shown in Table 1. The theoretical Ni content of the catalyst is 20%, the Al content is 42.4%, and the mass ratio of Ni/Al is 0.47, the others is nonmetal element, O. The Ni, Al content and the mass ratio of Ni/Al of the fresh catalyst is 20.5%, 41.7%, and 0.45, respectively, in agreement with the theoretical value, indicating that the impregnated combustion of nickel-containing materials are all loaded in the catalyst. The contents of Ni and Al in the catalyst decrease to 19.0% and 39.7%

respectively after 150 h reaction. After 450 h, the contents of Ni and Al decrease to 15.4% and 32.9%, respectively. It is concluded that as the reaction time is prolonged, the Ni and Al contents of the catalyst descend gradually, and nonmetal elements increase, which indicates indirectly that the amount of carbon deposition increases. The Ni/Al mass ratio of the catalyst after the reaction is still around 0.47, which is not dramatically different from that of the fresh catalyst. The results indicate that there is no Ni component loss during the reaction.

Table 1. Inductively coupled plasma atomic emission spectrometer results of catalyst.

Catalyst	Ni Relative Content/wt%	Al Relative Content/wt%	Mass of Ni/Al
(Theoretical value)	20	42.4	0.47
Cat-fresh	20.5	45.6	0.45
Cat-used-150	19.0	39.7	0.48
Cat-used-300	17.1	37.1	0.46
Cat-used-450	15.4	32.9	0.47
Cat-refreshed	20.1	44.7	0.45

2.3. Microstructure and Morphology of Catalyst

Table 2 shows the N₂ adsorption characterization results of the catalyst. The specific surface area and average pore volume of fresh catalyst is 167 m²·g⁻¹ and 0.278 cm³·g⁻¹, respectively, and the average pore size is 7.1 nm. The surface area of the catalyst changes a little after 150 h, while the specific surface area decreases significantly to 128 m²·g⁻¹ after 300 h, and the pore volume and pore size decrease observably, which indicates that the catalyst channels are blocked by carbon deposition. After 450 h, the average pore size of the catalyst is reduced to 4.8 nm, while the specific surface area and average pore volume increased to 134 m²·g⁻¹ and 0.219 cm³·g⁻¹. With increasing amount, carbon deposition from the surface of Ni particles adheres to the surface of the catalyst. The specific surface area, the average pore volume and pore size of the catalyst increased to 158 m²·g⁻¹, 0.273 cm³·g⁻¹ and 6.8 nm, respectively, in agreement with the fresh catalyst due to the removal of carbon deposition, and the blocked pore structure of the catalyst is recovered.

Table 2. Textural properties of catalysts.

Catalyst	S _{BET} (m ² ·g ⁻¹)	V _p (cm ³ ·g ⁻¹)	D _p (nm)
Cat-fresh	167	0.278	7.1
Cat-used-150	152	0.236	5.4
Cat-used-300	128	0.214	4.9
Cat-used-450	134	0.219	4.8
Cat-refreshed	158	0.273	6.8

The microstructure of the catalyst can be directly observed by TEM, which is helpful to understand the existence of carbon deposition. As shown in Figure 3, the fresh catalyst is in the form of granules with a diameter of 5–10 nm. Simultaneously, it has a uniform particle size and clear particles. After 150 h of methanation, the edge of the catalyst particles become blurred, indicating that a small amount of carbon is present on the catalyst surface [38]. When the reaction time increases to 300 h, flat carbon film comes into being on the edge of the sample, wrapping in the catalyst surface. However, after 450 h, the surface area of the catalyst continually increases, forming a multilayer carbon film, and the surface of the carbon film is no longer flat and superimposes on each other. After the regeneration process, the carbon species disappears, and the morphology of the catalyst is similar to that of fresh catalyst.

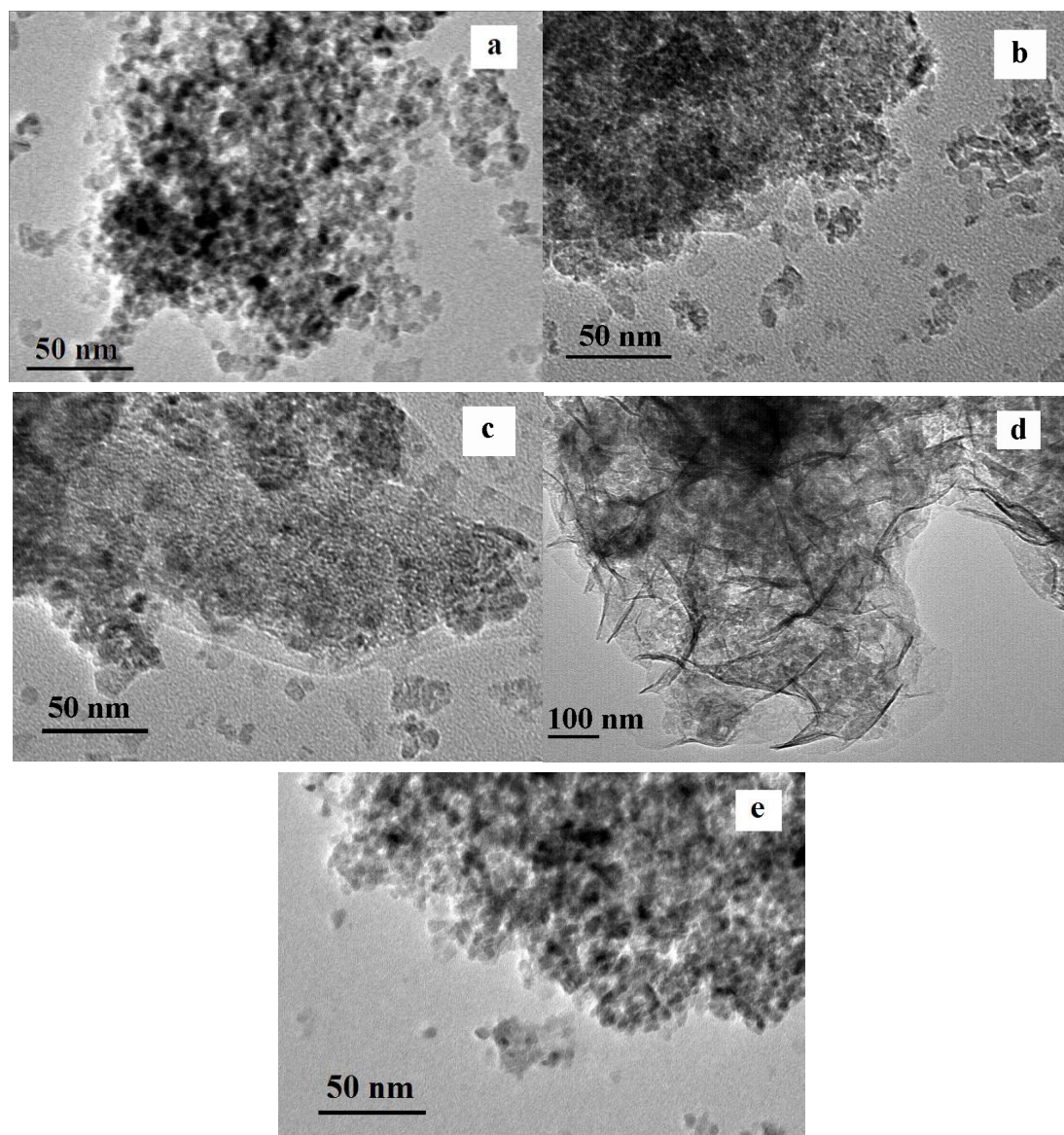


Figure 3. TEM of catalysts. (a) Cat-fresh, (b) Cat-used-150, (c) Cat-used-300, (d) Cat-used-450 and (e) Cat-refreshed.

2.4. Carbon Deposition Analysis of Catalyst

Previous studies have shown that the loss of weight in the Thermogravimetric analysis (TG) characterization of the catalyst after the methanation reaction is generally due to the oxidation of carbon deposition [39,40]. To obtain the carbon content of the catalyst, the Ni/Al₂O₃ catalyst involved in the different stages of the methanation reaction was characterized by TG in the CO₂ atmosphere. The results are shown in Figure 4. According to the figure, the fresh catalyst has almost no weight loss, that is, it does not decrease in quality caused by carbon deposition oxidation. The weight loss of the catalyst after the methanation reaction occurs above 280 °C, indicating that carbon deposition forms after the reaction. The carbon deposition capacity of the catalysts is 4.5%, 15.6% and 32.8% at 150 h, 300 h and 450 h, respectively. It can be seen that as the reaction time is prolonged, the amount of carbon deposition increases. Nevertheless, the deactivated catalyst is oxidized and regenerated, it does not significantly lose weight, manifesting that the carbon deposition on the catalyst is substantially removed by the carbon deposition burning process.

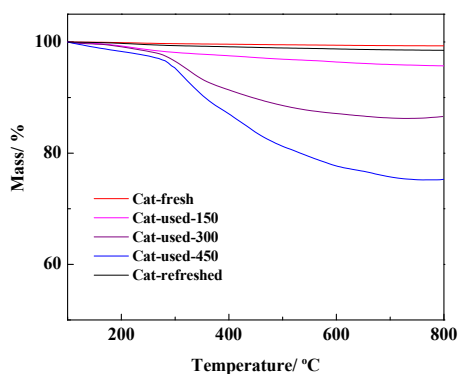


Figure 4. Thermogravimetric analysis of catalysts.

TPO is the programmed temperature oxidation, oxidation temperature of the carbon deposition can be obtained by it and the composition of carbon deposition can be deduced, the test results shown in Figure 5. It is observed that the catalyst has a significant oxidation peak at 230 °C, corresponding to the oxidation of Ni [41]. The reacted catalyst has an oxidation peak at 360 °C, 370 °C and 380 °C, corresponding to the oxidation of carbon deposition. Previous studies have shown that carbon deposition is divided into amorphous carbon, partially crystallized carbon and graphite carbon according to the degree of crystallization, their oxidation temperature is above 250 °C–450 °C [42,43], 450 °C–550 °C [44] and 550 °C [45], respectively. The temperature of the oxidation peaks shows that the carbon deposition on the catalyst is amorphous carbon. With the prolongation of methanation reaction time, the peak area of carbon deposition increases and the temperature of carbon deposition decreases. When the reaction time reaches 450 h, the temperature of carbon deposition peak decreases to 360 °C, which indicates that the amount of carbon deposition increases in the reaction, the interaction between carbon deposition and catalyst becomes weaker, and oxidation is more likely to occur.

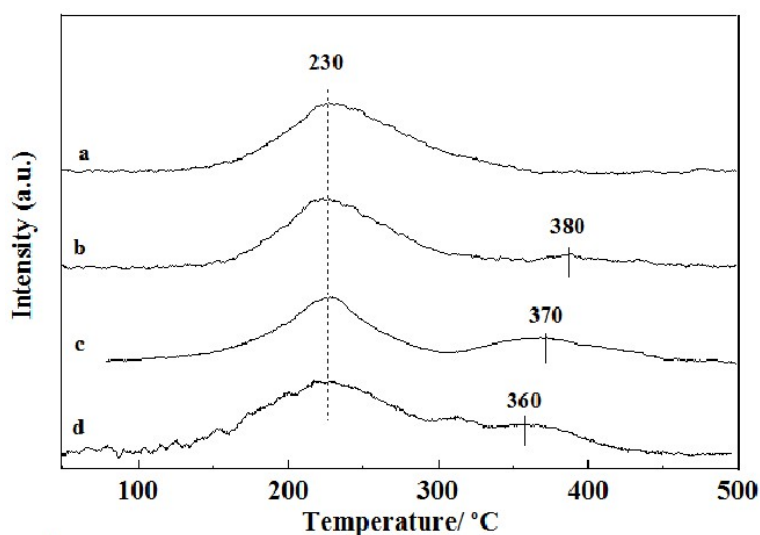


Figure 5. Temperature programmed oxidation of catalysts. (a) Cat-fresh, (b) Cat-used-150, (c) Cat-used-300 and (d) Cat-used-450.

2.5. H_2 Chemisorption Properties of Catalyst

The H_2 chemisorption results of the catalyst are shown in Table 3. It can be seen from the table that the surface area of the catalyst before reaction is $16.3 \text{ m}^2 \cdot \text{g}^{-1}$ and the metal dispersion is 2.45%. The surface area and metal dispersion of the catalysts were decreased after the reaction. After 450 h, the two decrease to $9.0 \text{ m}^2 \cdot \text{g}^{-1}$ and 1.35%, respectively, because parts of the Ni particles are coated with the carbon film during the reaction, blocking some of the catalyst channels and reducing the Ni active

sites exposed to the catalyst surface, metal surface area also decreases. The surface area and metal dispersion of the catalyst after the regeneration increase to $15.9 \text{ m}^2 \cdot \text{g}^{-1}$ and 2.40%, respectively, close to the fresh catalyst, which is due to the removal of the carbon deposition on the Ni surface during the regeneration process. The Ni phase can be re-exposed and subjected to H_2 chemisorption.

Table 3. Metallic surface area and metal dispersion of catalysts.

Catalyst	Metallic Surface Area/ $(\text{m}^2 \cdot \text{g}_{\text{metal}}^{-1})$	Metal Dispersion/%
Cat-fresh	16.3	2.45
Cat-used-150	15.3	2.29
Cat-used-300	12.6	1.89
Cat-used-450	9.0	1.35
Cat-refreshed	15.9	2.40

3. Discussion

Based on the evaluation and characterization of the $\text{Ni}/\text{Al}_2\text{O}_3$ catalyst prepared by the combustion method in the slurry-bed system, the causes of carbon deposition, the properties and morphology of carbon deposition, the relationship between the carbon deposition and the structure and activity of the catalyst were analyzed and discussed.

According to thermodynamics, in the methanation reaction and its reverse reaction, CO disproportionation and CH_4 decomposition occurred mainly in the low-temperature range of $<650 \text{ }^\circ\text{C}$ and the high temperature range of $>600 \text{ }^\circ\text{C}$ [46], respectively. However, because of the limitation of the boiling point of the liquid paraffin, the temperature of the slurry-bed methanation was low, generally below $350 \text{ }^\circ\text{C}$ ($280 \text{ }^\circ\text{C}$ in this experiment). Therefore, the carbon deposition is mainly produced by the disproportionation of CO in the slurry-bed methanation reaction system. Research has shown that carbon deposition generated by CO disproportionation is mainly amorphous carbon [47], which is consistent with the results of experimental observations.

As the reaction time was prolonged, the amount of catalyst deposits increased and the methanation activity decreased.

At the initial stage of carbon deposition, the disproportion of CO occurred on the surface of Ni active, resulting in carbon active precursor C^* . A small amount of C^* could be dissolved in the Ni to form Ni_3C species. However, the doping of Ni_3C caused the grain order of Ni to decrease. At this point Ni_3C in the Ni particles were not saturated, the catalyst surface was without carbon deposition precipitation, and its activity did not show a significant decline.

With the further accumulation of carbon deposition, the carbon species dissolved in the Ni particles was saturated, it precipitated from the Ni grains, and transferred to the Ni grain boundary. It was reported that the accumulation of carbon deposition occurred mainly in the Ni/carrier interface and the outer surface of Ni; the driving forces were the temperature gradient and the concentration gradient of carbon [41]. In the gas–liquid–solid three-phase reaction system of slurry-bed, there was a significant temperature gradient in the Ni/liquid interface due to the excellent heat transfer performance of the liquid phase; meanwhile, the weak polarity of liquid phase was similar to that of carbon, which corresponded to the like-dissolves-like effect. The combined action of temperature gradient and polarity matching led to the accumulation of precipitated carbon species in the Ni/liquid interface. Because of the low reaction temperature, carbon deposition did not form a relatively high degree of crystallinity of carbon species, such as carbon fiber, carbon tube, and even graphite carbon, but rather a less orderly film formed. The coating of the carbon film covered part of the Ni active site, blocking some of the catalyst channels, and hindering the gas phase mass transfer, finally causing the methanation activity to decrease.

When the carbon deposits continued to increase, the carbon film on the surface of the catalyst underwent deformation, crushing, stacking, and the morphology became broken and irregular.

Furthermore, it was gradually separated from the catalyst surface to form a multilayer three-dimensional carbon structure. As the Ni active center was further covered, the catalyst pores were further blocked, and the surface area of the active metal decreased, leading to a decline of methanation activity. At the same time, the appearance and increase of the irregular carbon structure on the catalyst surface increased the catalyst surface area.

Since the carbon deposition in the slurry-bed methanation system generated in the Ni/liquid interface rather than the Ni/carrier interface, no Ni particles fell off and pore structure was not destroyed. The carbon deposition can be removed by oxidative roasting to re-expose the active site, thus the blocked pore structure and the catalyst activity are recovered.

4. Experimental Section

4.1. Catalyst Preparation

The catalyst was prepared by impregnation-combustion method. Firstly, 12.4 g of nickel nitrate (>98.0%, Sinopharm Chemical Reagent, China) and 4.3 g of urea (A.R.; Tianjin Fengchuan Chemical Reagent, Tianjin, China) were dissolved in 10 mL distilled water. Then, 10 g of γ -Al₂O₃ (supplied by Zhengzhou Alumina Company, Zhengzhou, China) was slowly added into the solution and immersed for 24 h. After the impregnation, the suspension was poured into a ceramic evaporator and placed in a muffle furnace for several minutes at a temperature of 300 °C. After it had spontaneously burned, a catalyst precursor was obtained. Then, it was grounded to 80–100 mesh and reduced at 550 °C for 6 h with the gas $v(\text{H}_2)/v(\text{N}_2) = 4/1$ at a flow rate of 125 mL/min, the as-received sample was methanation catalyst, designated as Cat-fresh. The loading content of Ni on catalyst was 20 wt%.

4.2. Catalyst Activity Evaluation and Regeneration

2 g of catalyst and 120 mL of liquid paraffin (A.R.; Tianjin Kemiou Chemical Reagent Co.; Ltd., Tianjin, China) were added to a 250 mL autoclave (CJF-0.25, Dalian Tongda Reactor Factory, Dalian, China), then N₂ was introduced to sweep the air and enhance the pressure to 1.0 MPa, the feed gas was switched to 25% CO-75% H₂. The activity test was performed under the conditions of 280 °C, 1.0 MPa, and 3000 mL/(g·h) of space velocity. The off-gas was cooled by ethylene glycol at 1 °C to remove water vapor, then the gas was quantitatively analyzed on-line by a gas chromatography (7980A, Agilent Technologies, Inc., Santa Clara, CA, USA), which was equipped with three valves and four columns, and measured by the wet gas flowmeter (LML-1, Jinzhiye Instrument Equipment Co. Ltd., Beijing, China). Helium was used as carrier gas. Flame Ionization Detector (FID) detector was used to analysis of C₁₋₄ hydrocarbons, equipped with HP-AL/S column (30 m × 530 μm × 15 μm); Thermal Conductivity Cell Detector (TCD) detector equipped with Porapak-Q column, HP-PLOT/Q column (30 m × 530 μm × 40 μm), and HP- MOLESIEVE column (30 m × 530 μm × 25 μm) was used to analyze CO₂, and CO, CH₄, N₂.

By the end of the reaction, the catalyst was collected in the autoclave, and the liquid paraffin was removed from the surface of the catalyst by Soxhlet extractor, by using petroleum ether as solvent extraction. The extraction time was 200 h. The extracted catalyst was dried to remove the petroleum ether, collected as cat-used-t, t for the catalytic reaction time in units of h.

The catalyst after the reaction of 450 h was calcined at 400 °C for 4 h in air atmosphere to remove carbon deposition. It was then reduced in the same operation as the fresh catalyst, and designated as cat-refreshed. The regenerated catalyst was subjected to a slurry-bed methanation reaction under the same operating conditions as the fresh catalyst.

4.3. Characterization

X-ray diffraction (XRD) was used to characterize the catalyst by DX-2007 X-ray diffractometer (Haoyuan Instrument, Dandong, China), operating with CuK α radiation of wavelength $\lambda = 0.154056$ nm, Ni filter at 40 kV and 30 mA, the samples were scanned between 5°~85° at a rate of 8°/min.

Inductively Coupled Plasma Atomic Emission Spectrometer (ICP-AES) was performed on an iCAP 6300 (Thermo Fisher Scientific, Waltham, MA, USA) for the test of Ni and Al content of catalyst sample.

Nitrogen adsorption-desorption isotherms were carried out by 3H-2000PS2 automatic device (Beishide Instrument, Beijing, China). The samples were degassed at 30 Pa and 130 °C for 1 h. The N₂ was adsorbed at liquid nitrogen temperature and the specific surface area was calculated using the BET formula.

Transmission electron microscopy (TEM) (JEOL, Tokyo, Japan) was carried out by JEM-2100F field emission electron microscopy operated at 200 kV. The samples were dispersed in ethanol for 10 min, then the suspension was sprayed on a copper wire.

Thermogravimetric analysis (TG/DTG) was performed on STA409C (NETZSCH, Selb, Germany) integrated thermal analyzer at CO₂ atmosphere. The test temperature range was 100–800 °C, with the heating rate of 10 °C/min.

Temperature programmed oxidation (TPO) was performed on Aurochem II 2920 automatic instrument (Micrometrics Inc., Londonderry, NH, USA). About 40 mg catalysts were placed in a U-shaped quartz reaction tube. The temperature raised to 350 °C at a rate of 10 °C·min⁻¹ using He, kept blowing for 30 min at 350 °C. Subsequently, until it had cooled down to 50 °C, mixed gas of V(O₂)/V(He) = 1/9 was switched at the speed of 50 mL·min⁻¹. After the baseline is stabilized, the temperature was raised to 700 °C at a rate of 10 °C·min⁻¹, and the TCD was used to detect the exhaust gas signal.

H₂ chemisorption experiments were carried out with a Micrometrics Autochem II 2920 model multifunctional adsorption instrument (Micrometrics Inc, Londonderry, NH, USA). About 500 mg samples were placed in a U-shaped quartz reaction tube, at the atmosphere of V(H₂)/V(Ar) = 1/9 and the flow rate of 50 mL·min⁻¹, the temperature increased to 550 °C at the heating rate of 10 °C·min⁻¹ for 4 h. When cooled down to 120 °C, blowing 1 h at atmosphere, then continued to cooled to 50 °C. When baseline was stable, 15 pulses were performed (every pulse adsorption for 3 min at the atmosphere of V(H₂)/V(Ar) = 1/9). The pulse adsorption signal was detected by TCD.

5. Conclusion

The carbon deposition of Ni/Al₂O₃ catalyst, prepared by combustion method, was mainly due to the disproportionation of CO, which existed as amorphous carbon. The regularity of carbon deposition and the activity of the catalyst were as follows: (1) Initial stage of carbon deposition: carbon species first dissolved in the Ni grains, but did not form a carbon crystal, and the catalyst pore structure and catalyst activity changed slightly. (2) Carbon dissolved in the Ni was saturated, then it began to precipitate. Under the influence of the temperature gradient and like-dissolves-like effect of the paraffin, the carbon deposition on the Ni surface formed into the carbon film, blocking the pores and reducing the surface area of the active metal. (3) The carbon increased and gradually dissociated from the surface of the catalyst. The morphology of the carbon film became broken and irregular, and finally the multilayer three-dimensional carbon structure was formed. The catalyst pores were further blocked, but the specific surface area increased due to the appearance and increase of the irregular carbon structure. Active metal surface area and activity both decreased.

Additionally, the carbon deposition only covered the active site of the catalyst, no Ni particles fell off and the pore structure was not destroyed. Therefore, the carbon deposition could be removed without damaging the catalyst structure by oxidative calcination, the catalyst active site was re-exposed and the catalyst activity was recovered.

Author Contributions: F.M., K.J. and Z.L. conceived and designed the experiments; K.J. performed the experiments; K.J. and J.X. analyzed the data; P.L., K.Z., Z.L. and J.G. contributed reagents/materials/analysis tools; K.J. and F.M. wrote the paper.

Acknowledgments: This work was supported by the Natural Science Foundation of Shanxi Province (201801D121056).

Conflicts of Interest: The authors declare no conflict of interest.

References

1. Zhou, Q.; Liu, Q.; Shi, L.; Yan, Y.; Liu, Z. Behaviors of coking and radicals during reaction of volatiles generated from fixed-bed pyrolysis of a lignite and a subbituminous coal. *Fuel Process. Technol.* **2017**, *161*, 304–310. [[CrossRef](#)]
2. Zhang, S.; Xu, J.; Cai, Q.; Cui, Y. Production of aromatic hydrocarbons by hydrogenation-cocacking of bio-oil and methanol. *Fuel Process. Technol.* **2017**, *161*, 232–239. [[CrossRef](#)]
3. Cheng, C.; Shen, D.; Xiao, R.; Wu, C. Methanation of syngas (H₂/CO) over the different Ni-based catalysts. *Fuel* **2017**, *189*, 419–427. [[CrossRef](#)]
4. Ren, J.; Li, H.; Jin, Y.; Zhu, J.; Liu, S.; Lin, J.; Li, Z. Silica/titania composite-supported Ni catalysts for CO methanation: effects of Ti species on the activity, anti-sintering, and anti-coking properties. *Appl. Catal. B-Environ.* **2017**, *201*, 561–572. [[CrossRef](#)]
5. Tao, M.; Xin, Z.; Meng, X.; Bian, Z.; Lv, Y. Highly dispersed nickel within mesochannels of SBA-15 for CO methanation with enhanced activity and excellent thermostability. *Fuel* **2017**, *188*, 267–276. [[CrossRef](#)]
6. Jeong, Y.; Kim, I.; Kang, J.Y.; Jeong, H.; Park, J.K.; Park, J.H.; Jung, J.C. Alcohol-assisted low temperature methanol synthesis from syngas over Cu/ZnO catalysts: Effect of pH value in the co-precipitation step. *J. Mol. Catal. A Chem.* **2015**, *400*, 132–138. [[CrossRef](#)]
7. Zhang, C.; Chen, J.; Wen, Z. Assessment of policy alternatives and key technologies for energy conservation and water pollution reduction in China's synthetic ammonia industry. *J. Cleaner Prod.* **2012**, *25*, 96–105. [[CrossRef](#)]
8. Liu, G.; Larson, E.D. Comparison of coal/biomass co-processing systems with CCS for production of low-carbon synthetic fuels: Methanol-to-Gasoline and Fischer-Tropsch. *Energy Procedia* **2014**, *63*, 7315–7329. [[CrossRef](#)]
9. Yang, S.; Qian, Y.; Liu, Y.; Wang, Y.; Yang, S. Modeling, simulation, and techno-economic analysis of Lurgi gasification and BGL gasification for coal-to-SNG. *Chem. Eng. Res. Des.* **2017**, *117*, 355–368. [[CrossRef](#)]
10. Yang, S.; Liang, J.; Yang, S.; Qian, Y. A novel cascade refrigeration process using waste heat and its application to coal-to-SNG. *Energy* **2016**, *115*, 486–497. [[CrossRef](#)]
11. Li, S.; Ji, X.; Zhang, X.; Gao, L.; Jin, H. Coal to SNG: Technical progress, modeling and system optimization through exergy analysis. *Appl. Energy* **2014**, *136*, 98–109. [[CrossRef](#)]
12. Zhang, G.; Sun, T.; Peng, J.; Wang, S.; Wang, S. A comparison of Ni/SiC and Ni/Al₂O₃ catalyzed total methanation for production of synthetic natural gas. *Appl. Catal. A-Gen.* **2013**, *462–463*, 75–81. [[CrossRef](#)]
13. Kopyscinski, J.; Schildhauer, T.J.; Biollaz, S.M. Production of synthetic natural gas (SNG) from coal and dry biomass—A technology review from 1950 to 2009. *Fuel* **2010**, *89*, 1763–1783. [[CrossRef](#)]
14. Meng, F.; Li, X.; Li, M.; Cui, X.; Li, Z. Catalytic performance of CO methanation over La-promoted Ni/Al₂O₃ catalyst in a slurry-bed reactor. *Chem. Eng. J.* **2017**, *313*, 1548–1555. [[CrossRef](#)]
15. Meng, F.; Li, X.; Shaw, G.; Smith, P.; Morgan, D.; Perdjon, M.; Li, Z. Sacrificial carbon strategy toward enhancement of slurry methanation activity and stability over Ni-Zr/SiO₂ catalyst. *Ind. Eng. Chem. Res.* **2018**, *57*, 4798–4806. [[CrossRef](#)]
16. Meng, F.; Li, Z.; Liu, J.; Cui, X.; Zheng, H. Effect of promoter Ce on the structure and catalytic performance of Ni/Al₂O₃ catalyst for CO methanation in slurry-bed reactor. *J. Nat. Gas Sci. Eng.* **2015**, *23*, 250–258. [[CrossRef](#)]
17. Hui, W.; Zhang, J.-f.; Bai, Y.-x.; Wang, W.-f.; Tan, Y.-s.; Han, Y.-Z. NiO@SiO₂ core-shell catalyst for low-temperature methanation of syngas in slurry reactor. *J. Fuel Chem. and Technol.* **2016**, *44*, 548–556.
18. Zhang, J.; Bai, Y.; Zhang, Q.; Wang, X.; Zhang, T.; Tan, Y.; Han, Y. Low-temperature methanation of syngas in slurry phase over Zr-doped Ni/ γ -Al₂O₃ catalysts prepared using different methods. *Fuel* **2014**, *132*, 211–218. [[CrossRef](#)]
19. Gao, Y.; Meng, F.; Cheng, Y.; Li, Z. Influence of fuel additives in the urea-nitrates solution combustion synthesis of Ni-Al₂O₃ catalyst for slurry phase CO methanation. *Appl. Catal. A-Gen.* **2017**, *534*, 12–21. [[CrossRef](#)]
20. Gao, Y.; Meng, F.; Ji, K.; Song, Y.; Li, Z. Slurry phase methanation of carbon monoxide over nanosized Ni-Al₂O₃ catalysts prepared by microwave-assisted solution combustion. *Appl. Catal. A-Gen.* **2016**, *510*, 74–83. [[CrossRef](#)]

21. Ji, K.; Meng, F.; Li, Z. Ni-based catalysts prepared by impregnation combustion method for CO methanation in a slurry-bed reactor. *Asia-Pac. J. Chem. Eng.* **2016**, *11*, 151–157. [[CrossRef](#)]
22. Ke-Ming, J.; Fan-Hui, M.; Yuan, C.; Zhong, L. Solution combustion prepared Ni-based catalysts and their catalytic performance for slurry methanation. *Chin. J. Inorg. Chem.* **2015**, *31*, 267–274.
23. Keming, J.; Fanhui, M.; Yuan, G.; Zhong, L. Effect of fuel on structure and catalytic performance for slurry methanation over Ni-Al₂O₃ catalysts prepared by combustion method. *Chem. J. Chin. Univ.* **2016**, *37*, 134–141.
24. Bartholomew, C.H. Mechanisms of catalyst deactivation. *Appl. Catal. A-Gen.* **2001**, *212*, 17–60. [[CrossRef](#)]
25. Han, X.; Yang, J.; Guo, H.; Qin, Z.; Zhao, S.; Lu, Y.; Li, Z.; Ren, J. Mechanism studies concerning carbon deposition effect of CO methanation on Ni-based catalyst through DFT and TPSR methods. *Int. J. Hydrogen Energy* **2016**, *41*, 8401–8411. [[CrossRef](#)]
26. Helveg, S.; López-Cartes, C.; Sehested, J.; Hansen, P.L.; Clausen, B.S.; Rostrup-Nielsen, J.R.; Abild-Pedersen, F.; Nørskov, J.K. Atomic-scale imaging of carbon nanofibre growth. *Nature* **2004**, *427*, 426–429. [[CrossRef](#)]
27. La Cava, A.I.; Bernardo, C.A.; Trimm, D.L. Studies of deactivation of metals by carbon deposition. *Carbon* **1982**, *20*, 219–223. [[CrossRef](#)]
28. Ruckenstein, E.; Wang, H.Y. Carbon deposition and catalytic deactivation during CO₂ reforming of CH₄ over Co/γ-Al₂O₃ catalysts. *J. Catal.* **2002**, *205*, 289–293. [[CrossRef](#)]
29. Dabros, T.M.H.; Andersen, M.L.; Lindahl, S.B.; Hansen, T.W.; Høj, M.; Gabrielsen, J.; Grunwaldt, J.D.; Jensen, A.D. Hydrodeoxygenation (HDO) of aliphatic oxygenates and phenol over NiMo/MgAl₂O₄: reactivity, inhibition, and catalyst reactivation. *Catalysts* **2019**, *9*, 521. [[CrossRef](#)]
30. Gomes, R.; Costa, D.; Junior, R.; Santos, M.; Rodella, C.; Fréty, R.; Beretta, A.; Brandão, S. Dry reforming of methane over NiLa-based catalysts: influence of synthesis method and Ba addition on catalytic properties and stability. *Catalysts* **2019**, *9*, 313. [[CrossRef](#)]
31. Chen, L.; Hao, Z.; Yang, T.; Liu, W.; Zhang, D. Carbon deposition behavior of a Co–Ni aerogel catalyst in CH₄ oxy-CO₂ reforming using various types of reactors. *Int. J. Hydrogen Energy* **2014**, *39*, 15474–15481. [[CrossRef](#)]
32. Remiro, A.; Valle, B.; Aguayo, A.T.; Bilbao, J.; Gayubo, A.G. Operating conditions for attenuating Ni/La₂O₃–αAl₂O₃ catalyst deactivation in the steam reforming of bio-oil aqueous fraction. *Fuel Process Technol.* **2013**, *115*, 222–232. [[CrossRef](#)]
33. Li, Z.; Hu, X.; Zhang, L.; Liu, S.; Lu, G. Steam reforming of acetic acid over Ni/ZrO₂ catalysts: Effects of nickel loading and particle size on product distribution and coke formation. *Appl. Catal. A-Gen.* **2012**, *417–418*, 281–289. [[CrossRef](#)]
34. Li, J.; Zhou, L.; Li, P.; Zhu, Q.; Gao, J.; Gu, F.; Su, F. Enhanced fluidized bed methanation over a Ni/Al₂O₃ catalyst for production of synthetic natural gas. *Chem. Eng. J.* **2013**, *219*, 183–189. [[CrossRef](#)]
35. Zhang, J.; Xin, Z.; Meng, X.; Tao, M. Activity and stability of nickel based MCM-41 methanation catalysts for production of synthetic natural gas. *CIESC J.* **2014**, *65*, 160–168.
36. Panagiotopoulou, P.; Kondarides, D.I.; Verykios, X.E. Selective methanation of CO over supported Ru catalysts. *Appl. Catal. B-Environ.* **2009**, *88*, 470–478. [[CrossRef](#)]
37. Zhao, A.; Ying, W.; Zhang, H.; Ma, H.; Fang, D. Ni–Al₂O₃ catalysts prepared by solution combustion method for syngas methanation. *Catal. Commun.* **2012**, *17*, 34–38. [[CrossRef](#)]
38. Chen, X.; Tadd, A.R.; Schwank, J.W. Carbon deposited on Ni/CeZrO isooctane autothermal reforming catalysts. *J. Catal.* **2007**, *251*, 374–387. [[CrossRef](#)]
39. Hu, D.; Gao, J.; Ping, Y.; Jia, L.; Gunawan, P.; Zhong, Z.; Xu, G.; Gu, F.; Su, F. Enhanced Investigation of CO Methanation over Ni/Al₂O₃ Catalysts for Synthetic Natural Gas Production. *Ind. Eng. Chem. Res.* **2012**, *51*, 4875–4886. [[CrossRef](#)]
40. Guo, X.; Peng, Z.; Hu, M.; Zuo, C.; Traitangwong, A.; Meeyoo, V.; Li, C.; Zhang, S. Highly active Ni-based catalyst derived from double hydroxides precursor for low temperature CO₂ methanation. *Ind. Eng. Chem. Res.* **2018**, *57*, 9102–9111. [[CrossRef](#)]
41. Struis, R.P.; Schildhauer, T.J.; Czekaj, I.; Janousch, M.; Biollaz, S.M.; Ludwig, C. Sulphur poisoning of Ni catalysts in the SNG production from biomass: A TPO/XPS/XAS study. *Appl. Catal. A-Gen.* **2009**, *362*, 121–128. [[CrossRef](#)]
42. Le Valant, A.; Bion, N.; Can, F.; Duprez, D.; Epron, F. Preparation and characterization of bimetallic Rh-Ni/Y₂O₃-Al₂O₃ for hydrogen production by raw bioethanol steam reforming: influence of the addition of nickel on the catalyst performances and stability. *Appl. Catal. B-Environ.* **2010**, *97*, 72–81. [[CrossRef](#)]

43. Therdthianwong, S.; Srisiriwat, N.; Therdthianwong, A.; Croiset, E. Reforming of bioethanol over Ni/Al₂O₃ and Ni/CeZrO₂/Al₂O₃ catalysts in supercritical water for hydrogen production. *Int. J. Hydrogen Energy* **2011**, *36*, 2877–2886. [[CrossRef](#)]
44. Lu, Y.; Li, S.; Guo, L.; Zhang, X. Hydrogen production by biomass gasification in supercritical water over Ni/γAl₂O₃ and Ni/CeO₂-γAl₂O₃ catalysts. *Int. J. Hydrogen Energy* **2010**, *35*, 7161–7168. [[CrossRef](#)]
45. Zhang, L.; Li, W.; Liu, J.; Guo, C.; Wang, Y.; Zhang, J. Ethanol steam reforming reactions over Al₂O₃-SiO₂-supported Ni–La catalysts. *Fuel* **2009**, *88*, 511–518. [[CrossRef](#)]
46. Gao, J.; Wang, Y.; Ping, Y.; Hu, D.; Xu, G.; Gu, F.; Su, F. A thermodynamic analysis of methanation reactions of carbon oxides for the production of synthetic natural gas. *RSC Adv.* **2012**, *2*, 2358–2368. [[CrossRef](#)]
47. Bartholomew, C.H. Carbon deposition in steam reforming and methanation. *Catal. Rev.* **1982**, *24*, 67–112. [[CrossRef](#)]



© 2019 by the authors. Licensee MDPI, Basel, Switzerland. This article is an open access article distributed under the terms and conditions of the Creative Commons Attribution (CC BY) license (<http://creativecommons.org/licenses/by/4.0/>).